Review

International Journal of Modern Physics D
Vol. 23, No. 6 (2014) 1430012 (34 pages)

DOI: 10.1142/S0218271814300122

World Scientific
www.worldscientific.com

The accelerating universe and dark energy

Charles Baltay
Department of Physics, Yale University,
New Haven, CT 06520-8120, USA
charles.baltay@yale.edu

Received 10 March 2014
Accepted 28 March 2014
Published 12 May 2014

The recent discovery by Riess *et al.*[1] and Perlmutter *et al.*[2] that the expansion of the universe is accelerating is one of the most significant discoveries in cosmology in the last few decades. To explain this acceleration a mysterious new component of the universe, dark energy, was hypothesized. Using general relativity (GR), the measured rate of acceleration translates to the present understanding that the baryonic matter, of which the familiar world is made of, is a mere 4% of the total mass-energy of the universe, with nonbaryonic dark matter making up 24% and dark energy making up the majority 72%. Dark matter, by definition, has attractive gravity, and even though we presently do not know what it is, it could be made of the next heavy particles discovered by particle physicists. Dark energy, however, is much more mysterious, in that even though we do not know what it is, it must have some kind of repulsive gravity and negative pressure, very unusual properties that are not part of the present understanding of physics. Investigating the nature of dark energy is therefore one of the most important areas of cosmology. In this review, the cosmology of an expanding universe, based on GR, is discussed. The methods of studying the acceleration of the universe, and the nature of dark energy, are presented. A large amount of experimentation on this topic has taken place in the decade since the discovery of the acceleration. These are discussed and the present state of knowledge of the cosmological parameters is summarized in Table 7 below. A vigorous program to further these studies is under way. These are presented and the expected results are summarized in Table 10 below. The hope is that at the end of this program, it would be possible to tell whether dark energy is due to Einstein's cosmological constant or is some other new constituent of the universe, or alternately the apparent acceleration is due to some modification of GR.

Keywords: Cosmology; accelerating universe; dark energy.

PACS Number: 98.80.Es

1. Introduction

Cosmology, the study of the universe at its largest scales, is undergoing a period of intense development based on both rigorous theoretical and experimental input. The dominant force in cosmology is gravity. Einstein's theory of General

Relativity (GR), our modern theory of gravity, forms a solid theoretical underpinning of the recent progress. On the experimental side the discovery by Hubble of the expanding universe is the basis of the Big Bang model of a dynamic universe that allows a meaningful discussion of a beginning, and thus an age of the universe. The discovery of the Cosmic Microwave Background (CMB), the relic sea of photons left over from the early universe, further supports the Big Bang model. The realization from the rotation curves of galaxies that there is considerably more matter with attractive gravity, called dark matter, than we can see via electromagnetic radiation (the visible matter) complicates things. With attractive gravity between the components of the universe the expectation was that the expansion velocity of the universe, the so called Hubble velocity, would decrease with time, i.e. a decelerating universe. The recent discovery that the Hubble velocity is increasing with time, an accelerating universe, was an immense surprise. This led to the postulation of the existence of a new component of the universe, dark energy, with some very unusual properties, not the least among which is that it has, in some sense of the word, repulsive gravity that drives the acceleration. The best estimates that fit all of the presently existing data is that the energy/matter density of the universe is made up of:

Visible Matter	$\sim 1\%$
Dark Matter	$\sim 27\%$
Dark Energy	$\sim 72\%$

Since dark energy is by far the dominant constituent of the universe, and we know almost nothing about it, considerable attention in the astrophysical community is focused on learning more about its nature. The goal of this review article is to lay out the theoretical background of the cosmology of an expanding universe (Sec. 2), discuss the methods of measuring the cosmological parameters (Sec. 3), describe the evidence for the acceleration of the universe (Sec. 4), discuss the present experimental situation (Sec. 5), and to discuss the future experimental program to study the nature of dark energy (Sec. 6).

2. The Cosmology of an Expanding Universe

2.1. *Hubble's Law*

In studying the spectra of light emitted by distant galaxies Hubble noticed that spectral lines were displaced typically toward longer wavelength. He attributed this to the Doppler effect, according to which the wavelength of light emitted by a moving object is changed as

$$\lambda_{\text{observed}} = \lambda_{\text{emitted}} \quad \sqrt{(1 + v/c)/(1 - v/c)}.$$

Hubble further noticed that beyond our immediate neighborhood, the shift was always toward longer wavelength, i.e. distant galaxies were redshifted, where the redshift z is defined as

$$z = \frac{(\lambda_{\text{observed}} - \lambda_{\text{emitted}})}{\lambda_{\text{emitted}}}$$

implying that the distant galaxies were moving away from us with a velocity v, and furthermore the further the galaxy was from us, the faster it is moving, which led to Hubble's Law

$$v = Hd,$$

where d is the distance of the galaxy from the Earth and H is a constant, called Hubble's constant. This implies an expanding universe, as if in the aftermath of some initial explosion, usually referred to as the Big Bang. In this picture, the age of the universe takes on an explicit meaning and to a first approximation is the distance divided by the velocity of any given object, which from Hubble's law is

$$T = \frac{1}{H}.$$

This is usually referred to as the Hubble age. Since measurements of astronomical distances are notoriously difficult, Hubble's original estimate of H was quite large leading to an age of the universe younger then the estimates of the age of the earth. Modern measurements obtain a smaller value, the current best estimate being (see Table 7 below)

$$H = (70.8 \pm 1.4)\,\text{km/sec/Mpc},$$

where Mpc is short for Megaparsec. A measure of distance equal to 3.258 light years or 3.086×10^{16} meters.

The Hubble age would be the estimate of the age of the universe if the expansion velocity were constant over the entire age. Our present knowledge of the expansion history leads to an estimate of around 13.5 Billion Years.

2.2. *The expansion history of the universe*

In current discussions of cosmology the cosmological principle, the statement that the universe on its largest scales is homogeneous and isotropic, i.e. that it is the same at all points within the universe at any given time, is assumed. In such a universe, distances can be expressed in terms of a scale factor $a(t)$ such that

$$r(t) = a(t)r_0,$$

where $r(t)$ is the distance between any two points at a time t and r_0 is that distance today. With this definition $a(t) = 1$ today, was less then 1 in the past, and will be larger then 1 in the future.

In such a homogeneous, isotropic, expanding universe with a scale factor $a(t)$, the most general metric is given by the Robertson–Walker line element

$$ds^2 = a^2(t)\left[\frac{dr^2}{(l-kr^2)} + r^2 d\vartheta^2 + r^2 \sin^2\vartheta d\phi^2\right] - c^2 dt^2,$$

where k is the curvature. In order to obtain Einstein's equations that govern the expansion history of the universe, often called the Friedman equations, that is the equations that govern the development of the scale factor $a(t)$, we use the R–W metric in Einstein's field equation

$$R_{\mu\upsilon} - \frac{1}{2}g_{\mu\upsilon}R = \left(\frac{8\pi G}{c^2}\right)T_{\mu\upsilon} + g_{\mu\upsilon}\Lambda,$$

where $R_{\mu\upsilon}$ is the Ricci tensor, $T_{\mu\upsilon}$ is the momentum–energy stress tensor, Λ is the cosmological constant, and $g_{\mu\upsilon}$ is the metric.

The Ricci tensor can be written in terms of second partial derivatives of the metric with respect to the coordinates. The R–W metric elements can then be used to evaluate the $R_{\mu\upsilon}$ and then the left hand side of the field equation can be obtained. For a matter-dominated universe with negligible pressure the diagonal elements of $T_{\mu\upsilon}$ are $0, 0, 0, \rho$. Using this, the equations for $a(t)$ can be obtained:

$$\left(\frac{\dot{a}}{a}\right)^2 = \left(\frac{8\pi G}{3}\right)\left(\rho_0 a^{-3} + ka^{-2} + \frac{\Lambda}{3}\right),$$

$$\left(\frac{\ddot{a}}{a}\right) = -\left(\frac{4\pi G}{3}\right)(\rho + 3p) + \frac{\Lambda}{3},$$

where we used the energy density in an expanding universe in terms of today's energy density ρ_0 as $\rho = \frac{\rho_0}{a^3}$.

From the second equation, it is apparent that a positive acceleration can come from either a nonzero Λ or a negative pressure $p < -\rho/3$. The future development of the universe depends on the total energy density. The critical density is defined as the density that is the border between a closed (recollapsing) and an open (expanding forever) universe:

$$\rho_{\text{crit}} = \frac{3H_0}{8\pi G},$$

where H_0 is todays value of the Hubble constant. It is also convenient to define the energy density in terms of the critical density

$$\rho_0 = \Omega_m \rho_{\text{crit}},$$

and similarly define the energy density in the curvature term and the cosmological constant term, meant to be todays values, as

$$\Omega_m = \left(\frac{8\pi G}{3H_0^2}\right)\rho_0,$$

$$\Omega_k = \frac{k}{H_0^2},$$

$$\Omega_\Lambda = \frac{\Lambda}{3H_0^2}.$$

The equation of state parameter w is defined as the ratio of the pressure density p to the energy density ρ

$$p = w\rho.$$

The relationship between the redshift and the scale factor can be seen from the consideration that light emitted with a wavelength λ_{emitted} when the scale factor was $a(t)$ expands as the universe expands to an observed wavelength $\lambda_{\text{observed}}$ when the scale factor is 1, so that

$$\frac{\lambda_{\text{observed}}}{\lambda_{\text{emitted}}} = \frac{1}{a}.$$

From the definition of the redshift above, we have $\lambda_{\text{observed}}/\lambda_{\text{emitted}} = 1 + z$, so we have

$$a = \frac{1}{(1+z)}.$$

Putting all of these definitions together, we have the equation for the evolution of the scale factor, usually called the Friedman equation, for a matter-dominated universe as

$$\left(\frac{\dot{a}}{a}\right)^2 = H^2(t) = H_0^2[\Omega_m(1+z)^3 + \Omega_k(1+z)^2 + \Omega_\Lambda],$$

with the realization that $\dot{a}/a = v/d = H(t)$. The above is for a matter-dominated universe. If radiation with a pressure $p = 1/3\rho$ is to be included the term $\Omega_r(1+z)^4$ must be added, where Ω_r is the energy density in radiation, which falls off like $1/a^4$ since the number density of photons falls off like $1/a^3$ and the photon energy decreases like $1/a$ as the universe expands. If a component with negative pressure $p = w\rho$ is to be included where $w < 0$, (such a component is referred to as dark energy), then a term $\Omega_{\text{DE}}(1+z)^{3(1+w)}$ must be added.

$$\left(\frac{\dot{a}}{a}\right)^2 = H^2 = H_0^2[\Omega_r(1+z)^4 + \Omega_m(1+z)^3 + \Omega_{\text{DE}}(1+z)^{3(1+w)} + \Omega_k(1+z)^2 + \Omega_\Lambda].$$

2.3. *The growth of structure*

Superimposed on a homogeneous universe described in the section above, there are inhomogeneities whose origins are quantum fluctuations in the very early universe, amplified by the process of inflation. These inhomogeneities are the origins of the large scale structure that is seen today. The time dependence of the growth of structure in the universe is expressed in terms of the growth of structure parameter,

often called the density contrast, $g(r,t)$, and defined in terms of the matter density $\rho(r,t)$ as

$$g(r,t) = \frac{(\rho(r,t) - \rho_{\rm ave})}{\rho_{\rm ave}}.$$

Now consider a local region where we write the mass excess $g(r,t)$ as $g(t)$

$$\rho(t) = \rho_{\rm ave}(1 + g(t)).$$

An expression for the evolution of the excess $g(t)$ can be derived from GR as

$$\ddot{g} + 2H_0 E(z)\dot{g} = 4\pi G\rho g,$$

where $E(z) = [\Omega_m(1+z)^3 + \Omega_{\rm DE}(1+z)^{3(1+w)} + \Omega_k(1+z)^2 + \Omega_\Lambda]^{1/2}$.

Integrating this equation yields a solution that to a very good approximation can be written as[3]

$$g(z) = g(z=0)\exp\left[\int (1+z)^{-1}(\Omega_m(z))^{\Upsilon} dz\right],$$

where Υ is a parameter defined by GR and is to a good approximation

$$\Upsilon = 0.55 + 0.05[1 + w(z=1)].$$

Measurements of the growth of structure often use the two point correlation function $\xi(r)$, which is the probability of finding a pair of galaxies separated by a distance r. Analyses are often carried out in terms of the fourier transform of the two point correlation function, called the Power Spectrum $P(k)$

$$P(k) = \int \xi(r) e^{i\boldsymbol{k}.\boldsymbol{r}} d^3r,$$

where $k = 2\pi/s$ and s is the distance scale, usually expressed in units of Mpc/h. The Power spectrum can be related to the cosmological parameters by adopting some model of the growth of structure. The presently favored model is the Concordance Model, often referred to as the ΛCDM (Lambda Cold Dark Matter) model where Λ signifies a nonvanishing cosmological constant (dark energy) and CDM signifies that the majority of dark matter is nonrelativistic and therefore clusters under the influence of gravity. Another important parameter is σ_8, the amplitude of the power spectrum at the 8 Mpc/h scale. Both weak lensing (WL) and galaxy clusters, discussed below, measure the power spectrum and are thus sensitive to this parameter.

2.4. *Distances in an expanding universe*

Distances in an expanding universe are complicated. There is now experimental evidence from CMB measurements that the universe is flat, with a curvature $k = 0$, to a one percent precision. We will therefore discuss here the special case of distances in a spatially flat expanding universe. We start with the Robertson–Walker metric

with $k = 0$ and consider a ray of light moving in a straight line with $d\vartheta = 0$ and $d\phi = 0$. The R–W metric then reduces to

$$ds^2 = a^2 dr^2 - c^2 dt^2,$$

for light $ds^2 = 0$, so we have $dr = cdt/a$ and integrating

$$r = \int \frac{cdt}{a} = c \int \left(\frac{1}{a\dot{a}}\right)\left(\frac{da}{dz}\right) dz,$$

now since $a = 1/(1+z)$, $da/dz = -a^2$, and the integral becomes

$$r = c \int \frac{a}{\dot{a}} dz,$$

from before we had the equation for $(\dot{a}/a)^2$, which we can write as

$$\left(\frac{\dot{a}}{a}\right) = H_0 E(z),$$

with

$$E(z) = [\Omega_m (1+z)^3 + \Omega_{\rm DE}(1+z)^{3(1+w)} + \Omega_\Lambda]^{1/2},$$

we can then write the integral as

$$r(z) = \left(\frac{c}{H_0}\right) \int \frac{dz}{E(z)}.$$

This $r(z)$ is called the comoving distance.

(a) The angular size distance d_A is defined by considering the angle ϑ subtended at the observer by an object of diameter D at a redshift z, that is

$$\vartheta = \frac{D}{d_A}.$$

Since the light was emitted from the object in the past when the scale factor was a, the angle ϑ was determined at that time so the distance was $a(t)r(z)$, and since $a = 1/(1+z)$, the angular size distance is $r(z)/(1+z)$,

$$d_A = \left(\frac{1}{1+z}\right)\left(\frac{c}{H_0}\right) \int \frac{dz}{E(z)}.$$

(b) The Luminosity distance d_L is defined by considering the flux L, observed on Earth, for an object with intrinsic luminosity L_0, as

$$L = \frac{L_0}{4\pi d_L^2},$$

where the flux is in joules/sec/m^2 and is E_γ times the number of photons/sec times $1/r^2$ and $E_\gamma = hc/\lambda$, the photon energy. Since E_γ is smaller by a factor of $a(t)$ at

the observer, and the no. of photons per second is smaller by a factor of $a(t)$ at the observer, then at emission, we have

$$L = \frac{a^2 L_0}{4\pi r^2} = \frac{L_0}{4\pi d_L^2},$$

so we get $d_L = (\frac{1}{a})r(z) = (1+z)r(z)$, and thus

$$d_L = (1+z)\left(\frac{c}{H_0}\right)\int \frac{dz}{E(z)}.$$

3. Measurement of the Cosmological Parameters

The cosmological parameters to be determined by experimental measurements are today's value of the Hubble constant H_0 and the other parameters that enter into the equations for the development of the scale factor or the growth of structure parameter, namely Ω_m, Ω_k, Ω_Λ, and w. The possibility that w varies with time is taken into account by the simple parametrizations $w = w_0 + w_a(1-a)$. There are four prominent methods of measuring the cosmological parameters discussed in the community. These are Type 1a Supernovae (SNe), Baryon Acoustic Oscillations (BAO), WL, and Galaxy Clusters and Redshift Space Distortions (RSD). Supernova was the technique that led to the discovery of the acceleration of the expansion of the universe and is perhaps still the most mature, but the other methods are increasingly catching up in precision. Given the systematic uncertainties of cosmological measurements and the fact that the different techniques have very different systematics, the techniques are not so much competing with each other as complementing each other. The supernova and the BAO techniques measure the history of the growth of space via the measurements of d_L and d_A, while WL and the galaxy cluster techniques measure the growth of structure via the measurement of $g(t)$. These quantities are interrelated by GR. A comparison between the supernova, the BAO, and the WL, galaxy cluster and RSD techniques provides a test of GR. The results of these measurements are of sufficient fundamental importance that all of the techniques should be pursued to their fullest capabilities. The techniques will be discussed in turn in more detail below.

3.1. *Type* 1*a supernovae*

Supernova explosions are the endpoints in the lifecycle of a star. Stars shine by nuclear fusion processes converting hydrogen into helium in a main sequence star and helium, carbon, etc. into heavier elements in later stages as a red giant star. The pressure of this hydrogen bomb like explosion is balanced by the gravitational collapse in a stable star. When the star runs out of fuel, the unbalanced gravitational force implodes and then blows up the star in a supernova explosion. These are called core collapse supernovae and include Type 1b, 1c, and Type II supernovae. Their luminosity varies depending on the mass of the star.

Type 1a supernovae have a somewhat different origin. A star must have a mass larger than the Chandrasekar mass of approximately 1.4 solar masses to have sufficient gravitational energy to cause a supernova explosion. Stars lighter than this fizzle out and turn into brown dwarfs. Some brown dwarfs are in binary systems with another star, sometimes with a gaseous giant star. The brown dwarf may accrete mass from its binary partner and thus increase in mass. As it reaches the Chandrasekar limit it goes supernova. Since these Type 1a supernovae all have approximately 1.4 solar masses, their intrinsic luminosities are quite uniform. Using some features of these supernovae such as the width of their light curve and their color, they can be corrected to have an intrinsic luminosity L_0 to a precision of $\sim$15% and can therefore be called "standard candles."[4,5]

The Type 1a supernova as standard candles can be used to measure the expansion history of the universe i.e. the plot of the scale factor of the universe when the supernova light was emitted versus the time in the past when the supernova explosion occurred.[6] This is done by measuring the apparent brightness L of the supernova and its redshift z. Comparing the apparent brightness to the presumably known intrinsic brightness of the supernova determines its distance and from the distance the time in the past when the supernova exploded can be inferred knowing the velocity of light. The redshift gives the scale factor of the universe at the time of the supernova explosion via $a(t) = 1/(1+z)$. Each supernova then yields a point in the $a(t)$ versus t plot, and a large sample of supernovae thus measure the expansion history of the universe.

Type 1a supernova increase rapidly in brightness after explosion, reaching a maximum or peak brightness about 20 days after explosion, and then fade away in another 40 days. The Type 1a's are distinguished from other types of supernovae by their characteristic spectrum with a prominent SiII absorption feature near 6100 Angstroms. After a supernova is detected and identified as a Type 1a, its brightness is measured in several filter bands with a two or three day cadence as it rises and fades away. A plot of the brightness versus time is called the lightcurve, one in each filter band. The brightness of the supernova is taken to be the brightness at peak, usually in the supernova rest frame blue (B) filter band. The measured brightness has to be calibrated using standard stars with known brightness in each filter band, and a number of corrections have to be applied. The width of the lightcurve relative to a "typical" supernova gives a stretch factor s, and the $(B-V)$ color gives a color c. The stretch and color corrections are then

$$m_B(\text{corrected}) = m_B(\text{measured}) + \alpha(s-1) - \beta c,$$

where m_B is the brightness measured in magnitudes defined below, and the stretch and color correction coefficients α and β are determined from a sample of nearby (low redshift) supernovae. One further correction has to be made to account for the shift in the rest frame B band with respect to the observer frame filter bands due to the redshift. Knowing the redshift of the supernova an interpolation between the

observer frame filter bands can be made (the so-called K corrections) to find the brightness corresponding to the rest frame B band.

The usual way to analyze and present the supernova data is to plot the observed apparent magnitude m_B of each supernova versus its redshift z. Such a plot is called a Hubble diagram. The magnitude is an inverse logarithmic measure of the brightness of an object defined in terms of the observed flux (photons/cm^2/sec) as

$$m_B = C - 2.5 \log_{10}(\text{flux}),$$

where m_B is the magnitude in the B filter band in the supernova rest frame and C is a calibration constant that depends on the sensitivity of the detectors, the extinction of the atmosphere and the color filters used. In practice, C is determined on any given night (calibrated) by measuring the magnitudes of standard stars with known magnitudes, such as Landolt standard stars, at the same time as the supernova is observed.

The apparent magnitudes can be expressed in terms of the intrinsic magnitude M of the Type 1a supernova and its luminosity distance as

$$m_B = M - 2.5 \log_{10} \left(\left(\frac{10\, pc}{d_L} \right)^2 \right),$$

where the intrinsic magnitude M is defined as the magnitude of a Type 1a supernova at a distance of 10 parsecs. The luminosity distance, discussed above, is

$$d_L = (1+z) \left(\frac{c}{H_0} \right) \int \frac{dz}{E(z)},$$

where $E(z)$ includes the dependence on the cosmological parameters

$$E(z) = [\Omega_m (1+z)^3 + \Omega_{\text{DE}} (1+z)^{3(1+w)} + \Omega_\Lambda]^{1/2}.$$

Thus any set of parameters define a curve in m versus z of the Hubble diagram. Each measured supernova provides a point, with some error bars, on this diagram. In this way, the sample of supernovae can be used in a fit to select the best fit curve, and thus the best fit values of the cosmological parameters. A typical Hubble diagram for Type 1a supernovae is shown in Fig. 1.

3.2. *Baryon acoustic oscillations*

BAO technique also measures the history of the expansion of the universe. While the supernova method measures the luminosity distance with standard candles, the BAO method measures the angular size distance with standard rulers in space. The standard rulers are provided by the expansion of acoustic waves in the dense early universe. Over-dense regions due to statistical fluctuations soon after the end of inflation propagate as pressure waves. The pressure driving these waves are provided by radiation pressure, that is the pressure of photons interacting with the baryonic matter. At the time of decoupling when the universe has cooled sufficiently that the photon no longer interact with the baryons the wave stalls and the wave

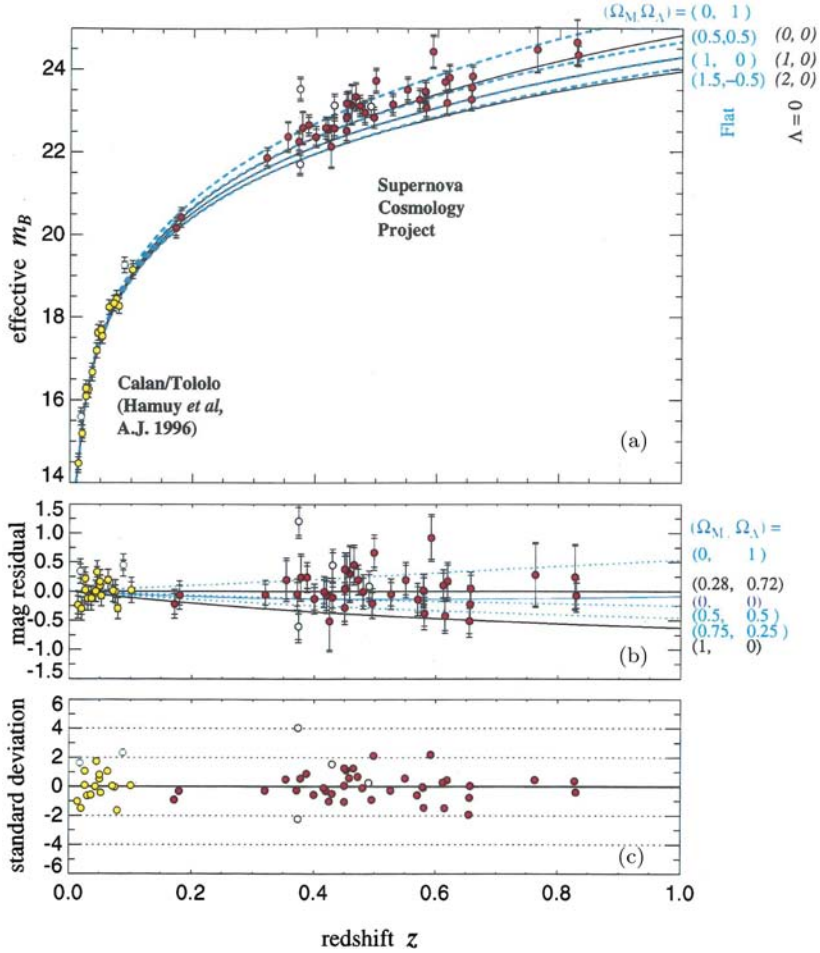

Fig. 1. (Color online) The Hubble diagram for Type 1a Supernovae, from Perlmutter *et al.*[2] The different curves represent different values of the cosmological parameters Ω_m and Ω_Λ, as labeled. The solid horizontal black line in the center of the lowest panel represents the best fit with $\Omega_m = 0.28$ and $\Omega_\Lambda = 0.72$.

front is frozen in the structure of baryonic matter in the universe. The velocity of propagation of these acoustic waves is known quite accurately to be $v = c/\sqrt{3}$ during the radiation-dominated era, and the time of decoupling has been measured to a 1 to 2% precision by the WMAP CMB experiments[42] to have occurred at $z = 1089 \pm 1$ or at a time $t = 379{,}000 \pm 8000$ years, so the diameter of the acoustic wave fronts is known to a high precision. In todays universe, this diameter is ~ 100 Mpc$/h$, where h is the Hubble constant in units of 100 km/sec/Mpc. With $h = 0.7$ the diameters are $D = 153 \pm 2$ Mpc and are the standard rulers used in the BAO method.

Experimentally, the BAO method measures the three-dimensional distribution of galaxies by measuring the right ascension, declination, and redshift of a large

number of galaxies. The large scale of the diameter of the acoustic wave fronts requires such a spectroscopic survey be carried out over huge portions of space over a sizeable range of redshifts. There are a large number of spherical wave fronts at any given z on top of a uniform background galaxy distribution. The two point correlation function of the distances between pairs of galaxies has a statistical distribution with a peak at the BAO scale at any given redshift. The first observation of the BAO scale[7] is shown in the plot of the two point correlation function versus pairwise galaxy separation in Fig. 2.

At any given redshift there are two independent pieces of information: the angular size $\Delta\vartheta$ transverse to the line of sight and Δz along the line of sight, as shown in the sketch of Fig. 3. Knowing the diameter D of the spherical wave front, the line of sight Δz provides a measure of the Hubble constant

$$H(z) = \frac{c\Delta z}{D}$$

and $\Delta\vartheta$ gives a measure of the angular size distance d_A at a range of redshifts z

$$d_A = \frac{D}{\Delta\vartheta}.$$

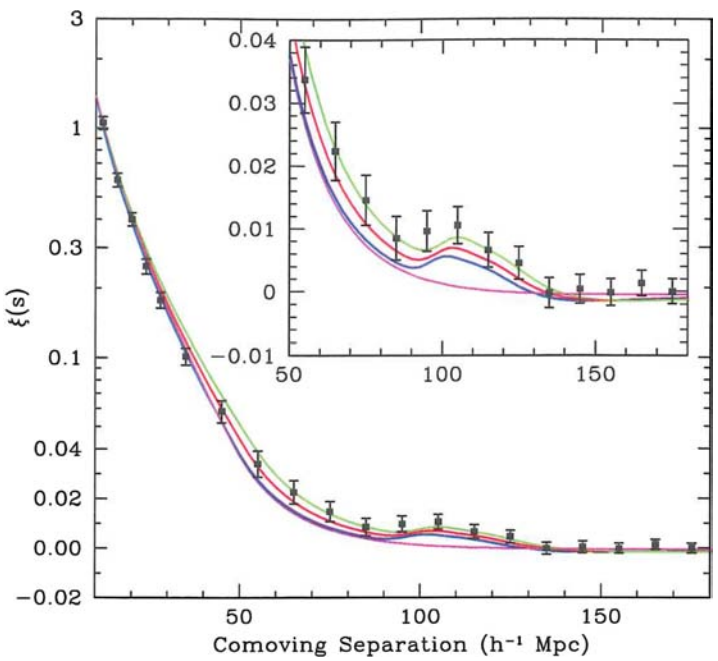

Fig. 2. First observation of the BAO scale, from Eisenstein *et al.*[7] At any given redshift, there are two independent pieces of information: the angular size $\Delta\vartheta$ transverse to the line of sight and Δz along the line of sight, as shown in the sketch of Fig. 3. Knowing the diameter D of the spherical wave front the line of sight Δz provides a measure of the Hubble constant.

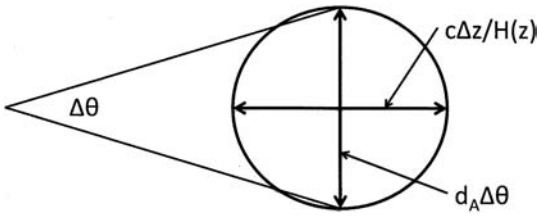

Fig. 3. Sketch showing the transverse size and the size along the line of sight of a BAO wave front.

The angular size distance, defined above, depends on $E(z)$ which in turn depends on the cosmological parameters. Thus a measurement of d_A as a function of redshift yields a measurement of the cosmological parameters.

The acoustic wave front expands as the universe expands from the time of decoupling to the present time. However the galaxies in this wave front have small peculiar velocities with respect to their uniform Hubble velocities. These peculiar velocities will cause the wave front to become fuzzy, smearing out the BAO scale measurement. An ingenious new method called reconstruction[8,9] ameliorates this problem. Having a measure of these peculiar velocities today, the clock can be run backwards and the galaxy positions can be extrapolated back to reduce the spread of the wave front. This method works remarkably well. Figure 4 shows a typical wave front before and after reconstruction. The improvement in the definition of the BAO scale measured experimentally in the SDSSII BAO survey is shown in Fig. 5. Reconstruction improves the precision of the measurement of the BAO scale by almost a factor of two.

3.3. *Weak lensing*

According to GR mass deflects light. Thus light from a distant background object is deflected by a large foreground mass, an effect called gravitational lensing. If the light passes near a very large mass, the image of the background object can be split

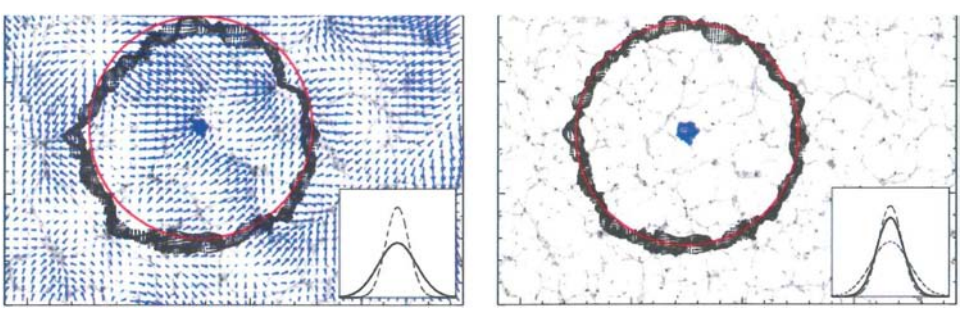

Fig. 4. A simulated BAO wave front before (left) and after (right) reconstruction, from Padmanabhan *et al.*[9]

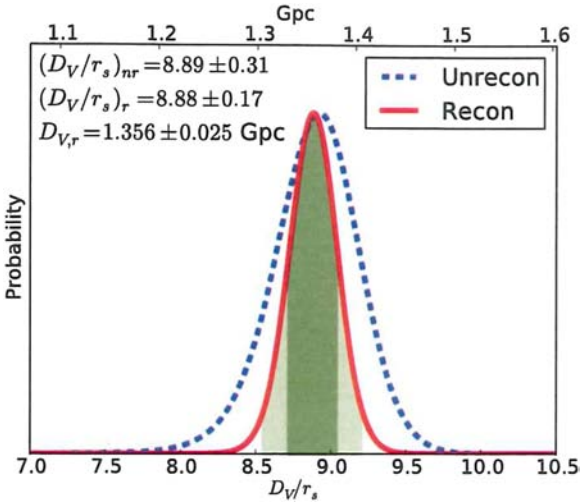

Fig. 5. (Color online) Precision in measuring the BAO feature before (blue dashed line) and after (solid red line) reconstruction, from Padmanabhan *et al.*[9]

into two or more distinct images, referred to as strong lensing. WL is when the lensing mass is more modest and the image of the background object is not split but is merely distorted. In the lensing of a distant galaxy by foreground galaxies, the distortion of the image of the galaxy is typically similar to the natural size of the galaxy image. It is thus hard to distinguish a spherical galaxy distorted into a more elliptical shape from an unlensed elliptical galaxy. There is power, however, in a statistical analysis. The direction of the distortions due to a foreground mass will be correlated in the form of circles around the lensing mass. It is unlikely that elliptical galaxies will be lined up with their major axes forming circles. Thus WL patterns at different redshifts can be used to measure the lumpiness, or the growth of structure parameter $g(z)$ discussed in Sec. 2.2 above as well as measuring the expansion history. GR relates the growth of structure parameter to the cosmological parameters, as

$$g(z) = g(z=0)\exp\left[\int (1+z)^{-1}(\Omega_m(z))^{\Upsilon} dz\right],$$

where $\Omega_m(z) = \Omega_m(0)(1+z)^{3(1+w)}$, so that Ω_m, w and Υ can be determined from a large WL survey.

WL, as well as galaxy clusters discussed in Sec. 3.4 below, are also sensitive to the amplitude (or normalization) of the matter power spectrum at a scale of 8 Mpc/h, usually called σ_8.

WL is the most challenging of the methods discussed so far. The tiny distortions in the shapes of galaxies by gravitational lensing are similar in size to the noise introduced by aberrations, slight vibrations, varying point spread functions etc.

especially with ground based telescopes. The importance of WL is however enhanced by the fact that WL measures the evolution of the growth of structure parameter $g(t)$ while supernovae and BAO measure the history of the scale factor $a(t)$. These are related by GR. Thus comparing the results of the three methods constitutes a check of GR. Another way to check the validity of GR is to write the Friedman–Robertson–Walker metric as

$$ds^2 = (1 + 2\Psi)dt^2 - a^2(t)(1 - 2\phi)d\mathbf{r}^2.$$

WL is sensitive to deviation of the potentials Ψ and ϕ from the predictions of GR (see discussion of Simpson *et al.*[10] in Sec. 5 below).

3.4. *Galaxy clusters and redshift space distortions*

3.4.1. *Galaxy clusters*

The attractive gravitational forces are pulling galaxies together to form galaxy clusters. Galaxy clusters are the largest observable structures in the universe. The presence of dark energy with repulsive gravity is slowing this process down. Thus the rate of cluster formation has information about dark energy. Cluster counting had some early successes in providing hints that the matter density Ω_m was less than one.[11,12] In recent years, due to larger and more sensitive cluster surveys, especially in X rays, and improved theoretical N body simulations, the capabilities of galaxy clusters to probe the cosmological parameters are improving rapidly. Interesting results have been recently obtained from X ray data from the ROSAT and Chandra space missions. Several methods have been used to obtain cosmological information from X ray data.

One method uses counting the number of clusters in a given mass range as a function of redshift. The main challenge in this method is getting the cluster mass from the cluster observables. In X rays the main observables are the total X ray luminosity, the cluster temperature and the X ray surface brightness. The mass is given mostly by the temperature, which is typically in the 5 to 15 KeV range, with small corrections from the other observables. The evolution of the cluster counts with redshift is sensitive to both the growth of structure and the evolution of space, which in turn are sensitive to the cosmological parameters.

Another method that has been used recently is measuring the baryon fraction in large luminous clusters. The baryon fraction f_b is the mass in baryons divided by the total mass of the cluster and is given by

$$f_b = \Upsilon(m, z)\frac{\Omega_b}{\Omega_m},$$

where $\Upsilon(m, z)$ is a correction factor, typically within 10% of unity, Ω_b is the baryon density in units of the critical density, and Ω_m is the matter density, including baryons, cold dark matter, and possibly neutrinos. In these analyses the baryon density is taken as known from big bang nucleosynthesis, $\Omega_b h^2 = 0.0214 \pm 0.002$,

so a measurement of the baryon fraction provides a measurement of Ω_m. The redshift dependence of the baryon fraction is sensitive to the other cosmological parameters such as the dark energy equation of state parameter w. The baryon fraction is obtained from the cluster observables mentioned above. The total cluster mass comes from the temperature and the X ray surface brightness gives the electron density in the cluster which in turn is related to the mass in baryons. The inherent assumption here is that Ω_b and Ω_m in the clusters is the same as the overall Ω_b and Ω_m in the universe.

Since the details of galaxy and of cluster formation are not completely understood there are significant systematic uncertainties connected with estimating the cluster masses from the cluster observables and relating these to the cosmological parameters. The topic of galaxy clusters, however, is of great interest to Astrophysics, and a large literature exists on this topic (see Allen *et al.*[52] and references therein).

3.4.2. *Redshift space distortions*

As discussed above, Supernova and BAO measure the evolution of space while WL and galaxy clusters measure the growth of structure. The importance of making both types of measurements is that the two effects are connected by GR, and a comparison of the results of the two provides a check on the validity of GR. RSD is another method that is sensitive to the growth of structure. The method depends on the realization[13] that in addition to the smooth Hubble velocity Hr, galaxies have peculiar velocities, and the observed velocity will be

$$v_{\rm obs} = Hr + v_{\rm pec}.$$

In the vicinity of a large structure, the peculiar velocities will be correlated, pointing toward the structure. Thus superimposed on the spatial redshift distribution due to the Hubble flow there will be a distortion pattern from which the unevenness of the matter distribution can be deduced, hence RSD. Doing this at a range of wavelengths is thus a measure of the rate of growth of structure. However the analysis is quite complicated mathematically and is plagued by the usual uncertainties of galaxy and cluster formation. A large amount of theoretical work is concentrated on the RSD method,[14,15] and there is general optimism that RSD will be a significant contributor, along with WL and galaxy clusters, in measuring the growth of structure in the universe, but the exact precision achievable is not clear at this time.

The RSD measurements require precise measurements of the redshifts of a large number of galaxies, which is exactly what a BAO surveys do. Thus all spectroscopic BAO surveys will provide the data for an RSD analysis. For this reason, RSD will not be listed and discussed separately in the section on future experiments but an RSD analysis will accompany every spectroscopic BAO survey, the larger the BAO survey, the better for RSD.

4. Discovery of the Accelerating Universe

The discovery of the acceleration of the expansion of the universe used the supernova method described in Sec. 3.1 above. Two groups reported significant evidence indicating the effect essentially at the same time. Riess *et al.*[1] had a sample of 37 Type 1a supernova, 27 low redshift ones ($z < 0.1$) and 10 at higher redshift ($0.16 < z < 0.62$). Perlmutter *et al.*[2] had 60 Type 1a supernova, 18 low redshift ones ($z < 0.1$) and 42 at higher redshift ($0.18 < z < 0.83$). Both data sets indicated an accelerating expansion of the universe, earning the two groups the 2011 Nobel Prize. The Hubble diagram for the Perlmutter *et al.*[2] data is shown in Fig. 1, with the 60 supernovae shown with their error bars on the m_B versus z plot. There are curves on the Hubble diagram corresponding to various values of the cosmological parameters as discussed in Sec. 3.1 above. Fits were carried out assuming a flat universe with $\Omega_k = 0$, which implies $\Omega_m + \Omega_\Lambda = 1$, and an Ω_m with $w = 0$. With these assumptions, both groups fit to

$$E(z) = [\Omega_m(1+z)^3 + \Omega_\Lambda]^{1/2}.$$

The best fits were $\Omega_m = 0.24$, $\Omega_\Lambda = 0.76$ from Riess *et al.*[1] and $\Omega_m = 0.28$, $\Omega_\Lambda = 0.72$ from Perlmutter *et al.*[2] Errors on these numbers were not quoted by Riess *et al.*, and the errors were of the order of ± 0.1 from Perlmutter *et al.* Both groups excluded $\Omega_\Lambda = 0$, Riess *et al.* at the three standard deviation level and Perlmutter *et al.* at the 99% confidence level. From the equation for the acceleration of the expansion discussed in Sec. 2.2

$$\left(\frac{\ddot{a}}{a}\right) = -\left(\frac{4\pi G}{3}\right)(\rho + 3p) + \frac{\Lambda}{3} = H_0^2\left[-\frac{1}{2}\Omega_m(1+z)^3 + \Omega_\Lambda\right],$$

it is evident that these values of Ω_m and Ω_Λ imply a positive acceleration today when $z = 0$.

In the original papers of both groups, the results were interpreted as a nonzero value of Λ. However, looking at the equation for the acceleration, if there were some new component of the universe with a negative pressure $p < -1/3\rho$, that is with $w < -1/3$, there could be a positive acceleration even with $\Lambda = 0$. In that case, $E(z)$ would be

$$E(z) = [\Omega_m(1+z)^3 + \Omega_{\rm DE}(1+z)^{3(1+w)}],$$

where Ω_m stands for matter density with zero pressure and $\Omega_{\rm DE}$ stands for the new component with negative pressure, which has been dubbed dark energy. From GR, we have the requirement that Ω_Λ have negative pressure with $w = -1$. Thus $\Omega_{\rm DE}(1+z)^{3(1+w)}$ could stand for Ω_Λ with $w = -1$ and no z dependence. It has become customary to use the term dark energy for either a new component with $w < -1/3$ but not $w = -1$, or for a cosmological constant with $w = -1$. The cosmological constant energy density would be independent of the redshift z and would have a constant w, while a new component would have a z dependent energy density and have possibly a time or z dependent value of w. Thus a measurement

of the value of w can distinguish between these two possibilities and is therefore of a high priority.

5. The Present Experimental Situation

Following the discovery of the acceleration of the universe, a large number of surveys were initiated to study the acceleration of the universe and the nature of dark energy. Vigorous programs were undertaken using all of the techniques discussed in Sec. 3 above.

5.1. *Type 1a supernovae*

Several surveys of Type 1a supernovae were carried out. Table 1 summarizes the major surveys. There have been a number of smaller early surveys, such as the original surveys of Riess *et al.*[1] and Perlmutter *et al.*[2] Most of these have been collected and included in the Union2 data set of Amanullah *et al.*[16] There have also been several low redshift surveys ($z < 0.1$) with a total of ~ 120 supernova that have been used to anchor the Hubble diagram for the higher redshift surveys. These are also included in the Union2 and the SNLS data sets and fits. The ongoing low redshift surveys are summarized in Table 2 below.

All of these surveys confirm the discovery that the expansion of the universe is accelerating, ruling out a nonaccelerating universe and a zero cosmological constant with a very high level of confidence. A Hubble diagram from the Union2 compilation is shown in Fig. 6. All of the surveys are consistent with $w = -1$, assuming a constant w and a flat universe. None of the surveys are able to put a significant

Table 1. Summary of the major supernova surveys.

Survey	z range	No of SNe	Reference
ESSENCE	0.2–1.0	60	Wood–Vasey *et al.*[17]
SNLS	0.3–1.0	242	Conley *et al.*[18]
HST Riess *et al.*	0.5–1.4	35	Riess *et al.*[19]
HST Suzuki *et al.*	0.6–1.4	14	Suzuki *et al.*[20]
SDSS II	0.1–0.5	752	Campbell *et al.*[21]
Union2 Data Set	0–1.4	557	Amanullah[16]

Table 2. Low redshift supernova surveys.

Survey	Start date	End date	Telescope, Fraction of supernova time	Magnitude limit	Reference
PTF	September 2009	2012	Palomar Schmidt, 80%	20–21	Shrinivas *et al.*[22]
CSP2	2012	2017	DuPont 2.5 m	21	Contreras *et al.*[23]
LaSilla/QUEST	December 2011	2017	ESO Schmidt, 90%	21.5	Baltay *et al.*[24]
SkyMapper	2013	2017	Australian 1 m, 30%	19.5	Keller *et al.*[25]
PanSTARRS	2009	Unknown	PanStarrs1, 25%	22–23?	Kaiser *et al.*[26]

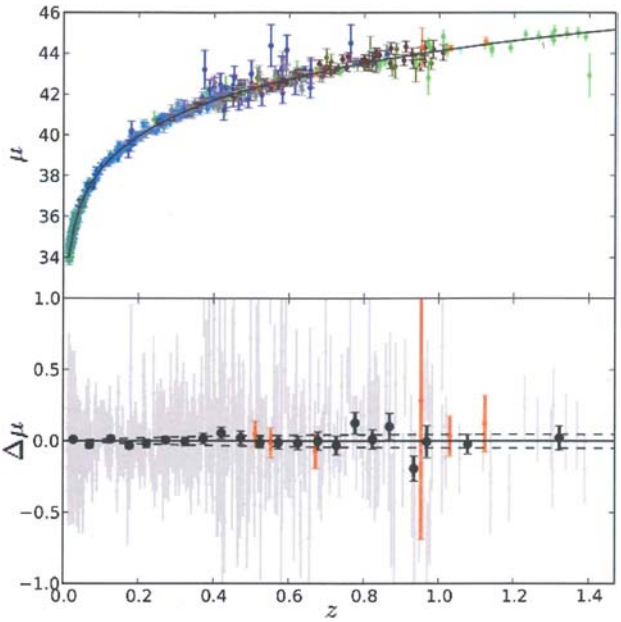

Fig. 6. (Color online) The Type 1a Supernova Hubble diagram for the Union2 data set, from Amanullah *et al.*[16] The gray vertical lines are individual supernovae, while the black points show the binned values. The orange points show new supernova reported for the first time in this paper.

limit on w_a, the variation of w with time, in the parametrization

$$w = w_0 + w_a(1 - a).$$

Very careful fits were carried out using the Union2 data set, Amanullah *et al.*,[16] which probably best represent the state of the art with supernovas. The fits assume a flat universe. Fixing $w = -1$, the best fit gives

$$\Omega_m = 0.274 \pm 0.04 \quad \text{and} \quad \Omega_\Lambda = 0.726 \pm 0.04.$$

With a flat universe, letting w vary but keeping it constant in time, and using the constraint from CMB, yields the best fit values

$$\Omega_m = 0.269 \pm 0.023, \quad \Omega_\Lambda = 0.731 \pm 0.023 \quad \text{and} \quad w = -0.999 \pm 0.08.$$

However it must be kept in mind that these results are based on the assumption that w is a constant. If w is allowed to vary with time, the constraints on w are much weaker.

5.2. *Baryon acoustic oscillations*

BAO method gained in credibility when the acoustic peak was first observed by the SDSSII collaboration in the Data Release 3 data, Eisenstein *et al.*[7] as shown in

Table 3. Summary of BAO surveys.

Survey	z Range	Area (sqdeg)	Galaxies	Reference
SDSSII	0.16–0.47	3816	46,748	Eisenstein *et al.*[7]
6dFGS	0.1	17,000	75,117	Beutler *et al.*[27]
WiggleZ	0.40–0.80	800	56,159	Blake *et al.*[28]
BOSS	0.40–0.70	3275	264,283	Anderson *et al.*[29]

Fig. 2. The peak, with a 3.4 standard deviation significance, was near the expected BAO scale of $100\,h^{-1}$ Mpc. Since then there have been a number of BAO surveys, summarized in Table 3.

All of the surveys confirm the BAO peak with increased significance at the BAO scale near $100\,h^{-1}$ Mpc. The best measurement of the BAO scale comes from the BOSS survey[29] which achieved a precision of 1.7%. The BAO scale measured by BOSS is shown in Fig. 7. All of the BAO measurements are in excellent agreement with each other and the combined measurement is in good agreement with the WMAP CMB results and the Supernova results.

5.3. *Weak lensing*

Before the last decade, there have been a dozen or so studies, looking at typically one or two square degrees of sky, looking at the systematic issues in measuring the distortion, or shear, in galaxies caused by WL. In the last decade, there have been a number of surveys looking for WL of distant galaxies by foreground galaxies in one or two hundred square degrees of sky. These recent surveys are summarized in Table 4 below.

The Sloane Digital Sky Survey (SDSS) used the 2.5 m telescope at Apache Point. The data from repeated observations of strip 82 were used, co-adding the repeated observations for a deep sample of galaxies, with magnitude limits of 23.5 in the r

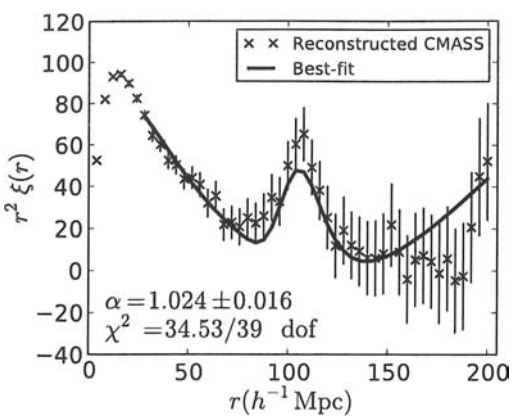

Fig. 7. The peak showing the BAO scale from the SDSSIII-BOSS survey, from Anderson *et al.*[29]

Table 4. Summary of recent WL surveys.

Survey	Telescope	Sky area	Redshift	References
SDSS	Sloane 2.5 m	275 sq deg	0.5 average	Huff *et al.*[30] Lin *et al.*[35]
CFHTLenS	CFHT 4 m	154 sq deg	0.2 to 1.3	Benjamin *et al.*[31] Kilbinger *et al.*[32] Kitching *et al.*[33] Simpson *et al.*[10]
DLS	Mayall 4 m Blanco 4 m	20 sq deg	Up tp 1.0	Jee *et al.*[34]

and 22.5 in the i filters. This sample had about 2.2 galaxies/square arcminute with a total of about two million galaxies with photometric redshifts with an average redshift of 0.5. Two WL analyses have been carried out using this sample of galaxies. Huff *et al.*[30] used a cosmic shear measurement out to angular separations of two degrees. Their results, assuming a flat ΛCDM model and combining with WMAP7 were $\sigma_8 = 0.784 \pm 0.027$ and $\Omega_m h^2 = 0.1303 \pm 0.0047$. These are a reduction of about 15% of the errors of WMAP7 alone. Lin *et al.*[35] analyzed 275 square degrees for distortions of the galaxy shapes due to cosmic shear, using the shear–shear correlation function and power spectrum. Their result was $\sigma_8 \Omega_m^{0.7} = 0.252 + 0.032/-0.052$.

The CFHTLenS survey used the 4 m Canada French Hawaii Telescope 154 square degree deep multicolor survey in five filter bands. Accurate photometric redshift and galaxy shape measurements were carried out. The sample contained 11 galaxies per square arcminute suitable for lensing studies, for a total of 6 million galaxies in the redshift range of 0.2 to 1.3. Four WL studies were done using this sample.

Benjamin *et al.*[31] present cosmological constrains using tomographic weak gravitational lensing over an angular range of 1 to 40 arcminutes in two broad redshift bins $0.5 < z < 0.85$ and $0.85 < z < 1.3$. For a flat ΛCDM model and a fixed $\Omega_m = 0.27$, they find the normalization of the power spectrum $\sigma_8 = 0.771 \pm 0.041$. Combining with WMAP7, the BAO results from BOSS, and the prior on the Hubble constant from the Hubble Space Telescope, they obtain the results $\sigma_8 = 0.802 \pm 0.013$ and $\Omega_m = 0.2762 \pm 0.0074$, an improvement of between 1.5 and 2 in the precision of the same results without the CFHTLenS data.

Kilbinger *et al.*[32] used 4.2 million galaxies with redshifts within 0.2 and 1.3 for a two-dimensional cosmic shear correlation function measurement over angular scales between 0.8 and 350 arcminutes. From their lensing data alone for a flat ΛCDM model they obtain $\sigma_8 \ (\Omega_m/0.27)^{0.6} = 0.79 \pm 0.03$. Combining with WMAP7, the BAO results from BOSS, and the prior on the Hubble constant from the Hubble Space Telescope, they obtain the results $\sigma_8 = 0.814 \pm 0.014$ and $\Omega_m = 0.283 \pm 0.001$. For a curved CDM universe model allowing dark energy they obtain $\sigma_8 = 0.83 \pm 0.04$ and $\Omega_m = 0.283 \pm 0.001$.

Kitching *et al.*[33] used this data set to carry out a three-dimensional cosmic shear analysis. In this analysis, galaxies are not binned in redshift but each galaxy enters with its individual redshift. With this approach, assuming a flat cosmology, a nonevolving dark energy equation of state (i.e. a constant w), and combining with WMAP7, they obtain $h = 0.78 \pm 0.12$, $\sigma_8 = 0.88 \pm 0.23$, $\Omega_m = 0.252 \pm 0.079$, and $w = -1.16 \pm 0.38$.

Simpson *et al.*[10] use cosmic shear tomography from the CFHTLenS survey combined with a RSD analysis using data from the WiggleZ and the 6dFGS surveys (see Table 3 above) to put constraints on deviations from GR. They obtain limits on the deviations from GR of the spatial and temporal gravitational potentials discussed in Sec. 3.3 above as

$$\frac{\Delta\phi}{\phi} = -0.05 \pm 0.30 \quad \text{and} \quad \frac{\Delta\Psi}{\Psi} = 0.05 \pm 0.25.$$

The Deep Lensing Survey (DLS)[34] employed weak gravitational lensing by large scale structures, often called a cosmic shear measurement. The survey used the 4 m Mayall telescope in the north and the 4 m Blanco telescope in the south to obtain deep images in four filter bands over five 4 degree fields (two in the north and three in the south). Photometric redshifts were used with a reach up to $z = 1$. The number of galaxies per square arcminute varied between 13 and 20 in the various fields, and a total of 1.2 million galaxies were used in the analysis. Their result from WL alone is $\sigma_8 = 0.868 \pm 0.071$ and $\Omega_m = 0.262 \pm 0.051$. Combining with WMAP7 reduces these errors to $\sigma_8 = 0.815 \pm 0.020$ and $\Omega_m = 0.278 \pm 0.018$.

5.4. *Galaxy clusters*

As mentioned in Sec. 3.4, above constraints on the cosmological parameters have been obtained from X-ray Cluster measurements with the ROSAT and Chandra X-ray space observatories. These results are summarized in a comprehensive review by Allen *et al.*[52] Of these, four papers report measurements of the dark energy equation of state parameter w. These are summarized in Table 5.

Allen *et al.*[36] and Ettori *et al.*[37] use the baryon fraction method, and Vikhlinin *et al.*[38] and Mantz *et al.*[39] use the evolution of cluster counts. All of the results listed in Table 5 assume a flat universe and a constant w, so that $\Omega_\Lambda = 1 - \Omega_m$. The results listed are using the galaxy cluster data only. These papers also quote results combining the cluster data with the results of other techniques such ac CMB, BAO

Table 5. Summary of measurements using galaxy clusters.

Reference	No. of clusters	Redshift range	σ_8	Ω_m	w
Allen *et al.*[36]	42	0.05–1.1		0.28 ± 0.06	-1.14 ± 0.31
Ettori *et al.*[37]	52	0.3–1.3		0.32 ± 0.05	-1.1 ± 0.65
Vikhlinin *et al.*[38]	86	0.05–0.55	0.81 ± 0.04	0.26 ± 0.08	-1.14 ± 0.21
Mantz *et al.*[39]	238	Up to 0.5	0.82 ± 0.05	0.23 ± 0.04	-1.01 ± 0.20

and Supernovae. Adding the cluster data to the others tend to improve the overall precision by anywhere from 10% to a factor of 1.5.

5.5. *Combined fits to the present data*

The measurements of the various cosmological parameters have been discussed in Secs. 5.1–5.4 above. Some of these are results of single measurements while others combine their results with various other methods. All of them make some assumptions such as a flat universe, constant equation of state parameter w, and so on. There have been a number of fits evaluating the cosmological parameters using all of the latest results combined.[18,28,29,40,41] The different fits use somewhat different combinations of input data, and make different model assumptions i.e. some assume a flat universe (keeping $\Omega_k = 0$), some allow Ω_k to vary, some keep w constant, some allow w to vary as $w = w_0 + w_a(1-a)$, etc. All of the fits are consistent within their errors and their assumptions.

The fits with the Union2 data set[16] combine the supernova data with the CMB results from WMAP[42] and the BAO results from SDSSII[7]. These fits in the Ω_m versus the Ω_Λ are shown in Fig. 8, and the fits in the w versus Ω_m plane are shown in Fig. 9. It is apparent from these figures that the errors from any one single technique are highly correlated in the parameters that they measure, but the correlation is quite different in the different techniques. Even though supernova and the BAO both measure the history of the expansion of space the relevant question is not which method gives the tightest errors. The two are complementary and their combination gives the best constraints on the cosmology. Hence the statement that it is crucial to pursue all techniques to the best sensitivity possible.

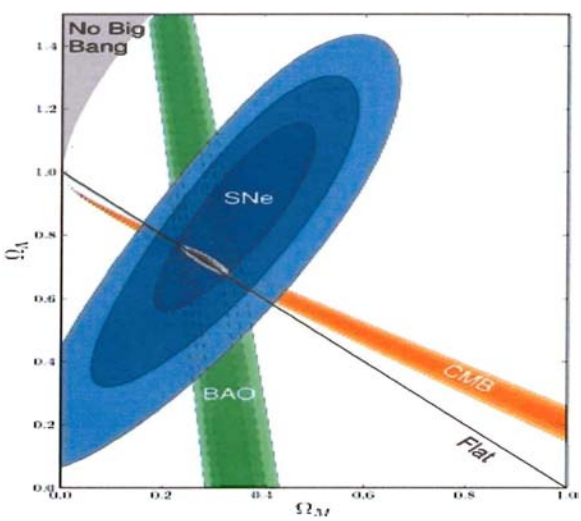

Fig. 8. Projection of the fit with the Union2 supernova data, CMB and BAO to the cosmological parameters in the Ω_m versus the Ω_Λ plane, from Amanullah *et al.*[16]

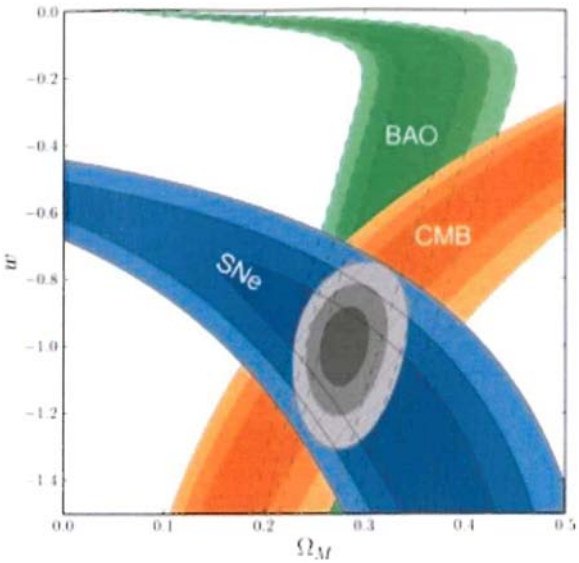

Fig. 9. Projection of the fit with the Union2 supernova data, CMB and BAO to the cosmological parameters in the w versus the Ω_m plane, from Amanullah *et al.*[16]

Table 6. Input used in the Anderson *et al.*[29] fit for the cosmological parameters.

Method	Survey	Reference
CMB	WMAP7 Data	Komatsu *et al.*[42]
BAO	SDSSII	Padmanabhan *et al.*[9]
BAO	BOSS	Anderson *et al.*[29]
BAO	6dFGS	Beutler *et al.*[27]
Supernova	SNLS3	Conley *et al.*[18]
H_0 Direct Measurement	HST	Riess *et al.*[43]

The most complete fit using the latest data is by Anderson *et al.*[29] where all of the parameters are allowed to vary. The inputs to this fit are summarized in Table 6.

The fits used the SNSL3 data set for supernova. The Union2 data set is sufficiently similar, so that using the Union2 data instead of or in addition to SNLS3

Table 7. Summary of the result of the fit to the cosmological parameters by Anderson *et al.*[29]

Parameter	Best fit value
Ω_m	0.270 ± 0.012
Ω_k	-0.010 ± 0.005
$\Omega_{\rm DE} = 1 - \Omega_m - \Omega_k$	0.740 ± 0.013
H_0(km/sec/Mpc)	70.8 ± 1.4
w_0	-0.93 ± 0.16
w_a	-1.39 ± 0.96

would not significantly change the results of the fit. The results of the most general fit letting all of the parameters vary are summarized in Table 7.

The fit summarized in Table 7 above represents the best estimates of the cosmological Parameters at the present time. These parameters are consistent with the acceleration of the universe being due to the cosmological constant introduced by Einstein with a constant $w = -1$, although with a sizeable error. However the time dependence of w at this stage is very poorly constrained and could provide surprises in the future. A great deal of experimental effort is planned to further improve our understanding of the acceleration of the universe and the nature of dark energy. These will be discussed in the next section.

6. The Future Experimental Program

Given the high level of interest in understanding the underlying reasons for the acceleration of the universe and the nature of dark energy, a vigorous program is planned worldwide to measure the cosmological parameters to a higher level of precision. In particular there is a focus on the measurement of the equation of state parameter w, which can distinguish between a cosmological constant ($w = -1$) or some other form of dark energy with $w < -1/3$ but not exactly -1. The present results, $w = -0.93 \pm 0.16$ (see Table 7) is consistent with the cosmological constant but higher precision may yet show a deviation from -1. The parameter w_a, indicating a time dependence of w, which would be inconsistent with a cosmological constant, is very poorly constrained by the present data.

It is interesting to point out that if it turns out that dark energy is due to a nonzero cosmological constant, a value of Ω_Λ in the vicinity of 0.7 would be implied. Such a small value of Ω_Λ would lead to one of the most dramatic inconsistencies in modern physics called the cosmological constant problem (see for example Weinberg[44] for a discussion of this issue). Modern field theory of particle physics predicts that the energy density of the vacuum contributes to the cosmological constant with a value 120 orders of magnitude larger than the experimentally observed value. Actually this problem would persist even if the dark energy turned out to be something else than the cosmological constant, with $\Lambda = 0$. Even though many theorists have tried, there is no explanation in sight to this fundamental disagreement.

There is also a realization that it is important to pursue all of the techniques of measuring the cosmological parameters. It is apparent from Figs. 8 and 9 that the supernova and the BAO have error bands that cross at an angle, and thus measuring both is quite important. It has also been pointed out above that Supernova and BAO measure the growth of space while WL and galaxy clusters measure the growth of structure. A comparison of these two should give an indication of whether there is a new component of the universe, like dark energy, or whether a modification of GR is the cause of the apparent acceleration of the universe.

There will still be improvements from the presently ongoing programs. LaSilla/QUEST, CSP2, SkyMapper and possibly PTF, will continue to increase

the sample of nearby supernovae, and SNfactory and PTF have yet to finish analyzing and publishing their large sample of nearby supernovae. SNLS and BOSS have so far published results from a part of their data, and both are continuing to analyze a considerably larger data set. These will further improve the precision of the results listed in Table 7.

There is a vigorous program, both ground based and space based, planned for the coming decade. Some of these, such as PanSTARRS1, DES, HSC, and HETDEX, are already, or about to be, operating. Some, such as LSST and EUCLID, are approved and in construction, while a few, such as DESI, PFS, and WFIRST, are still in the planning stage waiting for final approval. The major ground based programs are summarized in Table 8 and the space based missions are summarized in Table 9. References to these projects are given in the discussion of each project below. All of these programs have science objectives in addition to dark energy, but these will not be discussed here as they are beyond the scope of this review.

Table 8. Summary of the major ground based dark energy surveys.

Project	Telescope	Detector area	Start date	Techniques
PanSTARRS	1.8 m PanSTARRS Haleakala Hawaii	3.0 sq deg	2010	Supernova BAO WL
DES	4 m Blanco Cerro Tololo Chile	3.5 sq deg	2013	Supernova BAO WL
SuMIRe HSC + PFS	8.2 m Subaru Mauna Kea Hawaii	1.3 sq deg	2013 HSC 2018 PFS	Supernova BAO WL
HETDEX	9 m Hobby-Eberly McDonald Obs Texas	~ 1 sq deg	2014	BAO
DESI	4 m Mayall Tel Kitt Peak Arizona	7.0 sq deg	2018	BAO
LSST	8 m LSST Cerro Pachon Chile	9.6 sq deg	2020	Supernova BAO WL

Table 9. Summary of the space based dark energy missions.

Mission	Telescope	Detector area	Start date	Techniques
EUCLID	1.2 m	0.56 sq deg vis 0.55 sq deg NIR	2020	BAO WL
WFIRST	2.4 m	0.28 sq deg Vis-NIR	2022	Supernova BAO WL

6.1. *Ground based experiments*

6.1.1. *PanSTARRS*

PanSTARRS[26] is an ambitious project of the University of Hawaii Institute for Astronomy, expecting an array of four 1.8 m telescopes with a 3 deg^2 field of view camera each. Each camera will consist of a 64×64 array of CCD detectors, 600×600 pixels each for a total of 1.4 billion pixels per camera. The first telescope, PanSTARRS1, has been operating on Mount Haleakala in Hawaii since 2010. The remaining three telescopes are still in the future. PanSTARRS1 should be able to find thousands of supernovae up to a redshift of 0.8 or so.

6.1.2. *DES*

The DES (Dark Energy Survey)[45] is an imaging survey initiated by Fermilab, using the 4 m Blanco Telescope at the Cerro Tololo Observatory in Chile. The Camera, designed and built specifically for this project, has a 3 deg^2 field of view and consists of 62 CCD's with $2\text{K} \times 4\text{K}$ pixels each with 10 micron pixels, with a plate scale of 0.27 arcsec per pixel. The DES survey has been allocated 512 nights of telescope time over five years.

The supernova survey envisioned for DES is described in detail in Bernstein *et al.*[45] The supernova survey is expected to use 10% of the photometric observing time in addition to some nonphotometric time. The survey will cover five fields with 3 deg^2 each, revisited with a 5 to 10 day cadence. The estimate is that 4000 Type 1a's will be discovered with redshifts between 0.1 and 1.2, peaking around a redshift of 0.6. Photometric redshifts will be used, with 20% of the supernova looked at spectroscopically. The estimate is that the efficiency for Type 1 a's will be better than 95%, with a contamination of core collapse supernova at the few % level.

DES is planning a Wide Field survey of 5000 deg^2 in five filter bands (Gunn filters g, r, i, z, y) over five years with sensitivity to 24th mag. The expectation is a galaxy density of 12 well-measured galaxies per arcminute squared. A total of 30 million galaxies are expected at a redshift range of $0.5 < z < 1.5$. Photometric redshifts will be used with an estimated precision of $0.08(1+z)$. This sample will be used for both WL and the BAO surveys. For the BAO survey, which is essentially a redshift survey, the photometric redshift precision will not be sufficient to measure Δz's along the line of sight for the $H(z)$ measurement. The survey will rely on the angular size $\Delta\theta$ measurements in bins of redshift from 0.5 to 1.5, providing a measurement of the angular size distance d_A, from which the cosmological parameters can be obtained. For WL survey, the 0.27 arcsec per pixel plate scale will be sufficient to measure the distortions of the huge number of detected galaxies.

6.1.3. *SuMIRe*

The SuMIRe (Subaru Measurement of Images and Redshifts) project uses the 8.2 m Subaru telescope located at Mauna Kea in Hawaii. The ten year project will use

two powerful new instruments, HSC (Hyper Suprime Camera) for imaging and PFS (Prime Focus Spectrometer) for spectroscopy. Both instruments make use of WFC (Wide Field Corrector) optics to increase the telescope field of view to 1.3 deg^2. HSC is an imaging camera consisting of 104 CCDs with 2K $\times$ 4K 15 micron square pixels each. The plate scale will be 0.17 arcsec per pixel. PFS will be a fiber spectrometer with 2400 fibers positioned by a computer controlled robotic mechanism. The resolution will be $R = 2000$ to 5000 depending on the wavelength, and the wavelength range will be 0.38 to 1.3 microns. HSC is ready now and a five year imaging survey from 2013 to 2018 is planned. PFS is just starting construction and is expected to have first light in 2017, and a five year spectroscopic redshift survey is planned from 2018 to 2023. With the combination of the two instruments, dark energy surveys are envisioned using all three of the major methods (Supernova, BAO and WL).

The five year HSC imaging survey will include a wide survey of 1400 deg^2 with a limiting sensitivity of mag 26.5 in five filter bands for WL. Photometric redshifts will be used. An Ultra-Deep survey of 3 deg^2 will be carried out for Type 1a supernova to a limiting magnitude of 28. A total of 500 supernova are expected with redshifts up to 1.4.

The five year spectroscopic survey with the PFS spectrometer will constitute the BAO survey, with not all of the time dedicated to BAO. The BAO survey will cover 1500 deg^2, with an estimated 4 million galaxies, with a redshift range of $0.8 < z < 2.4$, using the OII doublet for the redshift measurement. The line sensitivity will be 5×10^{-17} ergs/sec/cm^2.

6.1.4. *HETDEX*

HETDEX (Hobby Eberly Telescope Dark Energy Experiment)[46] will use the 9.2 m Hobby Eberly telescope at the McDonald Observatory in Texas. The goal of the project is a BAO survey using the VIRUS spectrometer (Visible Integral field Replicable Unit Spectrometer) that will have 230 fibers in each of 150 spectrometer units for a total of 34,000 fibers. The fibers, however will not be moveable so that on any one exposure an estimated 1% of the fibers will have a galaxy in them.

For the BAO survey[46] the Lyman α line will be used to measure the redshifts. In a three year survey of 420 deg^2 with a total of 140 nights about one million galaxies in the redshift range of $1.8 < z < 3.7$ are expected.

6.1.5. *DESI*

DESI (Dark Energy Spectroscopic Instrument)[47] is a spectroscopic survey aimed at using the BAO method to study dark energy. The project will use the 4 m Mayall telescope at Kitt Peak with corrector optics, designed and built for this purpose, to enlarge the field of view of the telescope to 3 degrees in diameter. The focal plate, roughly a meter in diameter, will be located at the prime focus

of the telescope and will contain 5000 fibers. The positions of the fibers will be adjusted by a computer controlled robotic mechanism, moving them to the location of 5000 galaxies whose positions were obtained by a target survey previous to DESI operations. The fibers will be fed to a spectrometer room below the telescope that will house 10 spectrometers handling 500 fibers each. The wavelength range of the spectrometer detectors will be 360 nm to 980 nm and the resolution will be $R = \lambda/\Delta\lambda = 2000$ to 5500, depending on the wavelength.

The DESI plan is to cover 14,000 deg^2 in a five year survey. DESI will use three samples of galaxies to measure the BAO scale at different redshift ranges. The main sample will be 30 million Emission Line Galaxies (ELGs) in a redshift range of $0.7 < z < 1.7$, using the OII doublet at 3727 Å to measure the redshifts. A second sample will be five million Luminous Red Galaxies (LRGs) with redshifts up to 1.0, using the 4000 Å break to measure redshifts. The third sample will be about one million quasars in the redshift range $2.2 < z < 3.5$, using the Lyman α forest features to measure redshifts. The redshift resolution will have a precision of $0.001(1 + z)$, which is sufficient to measure the BAO scale both transverse to and along the line of sight to provide robust d_A and $H(z)$ measurements as described in Sec. 3.2 above as well as an RSD measurement.

6.1.6. *LSST*

The LSST (Large Synoptic Survey Telescope),[48] to be located at Cerro Pachon in Chile, is an approved project funded by the US National Science Foundation and the Department of Energy. The project will utilize an 8.4 m telescope, built for this purpose, with a 9.6 deg^2 field of view camera. The camera will consist of a mosaic of 200 CCD's with $4\text{K} \times 4\text{K}$ pixels each, with 10 micron square pixels and a plate scale of 0.1 arcsec per pixel. The strategy of the main survey that will occupy the majority of the projected 10 year lifetime of LSST is to use 15 sec exposures so that an 18,000 deg^2 area of sky can be covered repeatedly every few days. The science capabilities of such a program have been discussed in the LSST Science Book.

One of the original motivations for LSST was the study of WL as a probe of cosmology. In this context, LSST is immensely powerful, with a sky coverage of around 20,000 deg^2 and billions of galaxies observed. Not surprisingly, the ultimate quality of LSST WL will be determined on how well systematic effects can be controlled. Probably the most significant systematic effect will be the aberrations in the measurements of galaxy shapes due to the Point Spread Function (PSF) variations due to telescope and atmospheric effects. The shape distortions due to WL are at the sub-percent level, similar to the distortions due to the PSF. If the PSF were perfectly stable over both the area of the detector and in time, corrections for this systematic could be implemented. The variations of the PSF, especially those due to atmospheric effects in a ground based telescope, make these corrections especially challenging. Another systematic effect is due to the requirement that the redshifts of the galaxies have to be known to a sub-percent precision. Given

the large number of galaxies needed for WL studies, photometric redshifts have to be relied on. To achieve the required precision, Bernstein *et al.*[49] estimate that a calibration sample of 10^5 to 10^6 galaxies with spectroscopic redshifts will be needed to train and calibrate the photo z methods. Thus the results of the WL survey will depend on how well LSST will be able to control the systematic uncertainties.

LSST will also be able to carry out a sensitive BAO survey with the expected 10 Billion galaxies in a 20,00 deg^2 area of sky. A BAO survey is by necessity a redshift survey. With the large numbers of galaxies involved, photometric redshifts will have to be relied on, the limited precision of which will make the LSST BAO survey systematics limited. As discussed in Sec. 3.2 above, the BAO method allows both a transverse measurement of the BAO scale, which is a $\Delta\theta$ measurement, as well as a measurement along the line of sight, which is a Δz measurement. The estimate in the LSST Science Book is that the precision of photometric galaxy redshifts, of the order of $0.05(1+z)$, is not sufficient for the line of sight measurement. The proposed scheme then is to divide the data into 30 redshift bins from $z = 0.15$ to $z = 3.5$, in bins proportional to $(1 + z)$. The two point correlations in the angle between galaxies provides a measurement of the angular size distance in each redshift bin, which in turn leads to a measurement of the cosmological parameters. This should allow a BAO measurement competitive with the spectroscopic BAO surveys.

LSST will discover hundreds of thousands of supernovae during its 10 year observing period in a redshift range of 0.1 to 1.0, the exact number depending strongly on the selection and quality requirements imposed. Only a very few of these can be followed spectroscopically, so that photometric redshifts will have to be used. Thus the cosmological constraints from such a semi-infinite sample will be systematic limited. Also, as with any ground based supernova survey, the redshifts will be limited to around $z < 1$.

6.2. *Space based experiments*

6.2.1. *EUCLID*

EUCLID is a space mission of the European Space Agency (ESA), with an international collaboration. The mission design focuses on WL technique, with a strong BAO component, as described in the EUCLID Red Book.[50] The supernova technique has not been a design driver. The mission is based on a three mirror anastigmat telescope with a 1.2 m diameter primary mirror. The plan includes two imaging focal planes. The visible imager, covering a wavelength range of 550 to 900 nm, consists of 36 CCD's with $4\text{K} \times 4\text{K}$ pixels each, with a field of view 0.787×0.709 deg^2. The 10 micron pixels correspond to a plate scale of 0.10 arcsec per pixel. The near infrared (NIR) imager, covering from 920 to 2000 nm, consists of 16 HgCdTe detectors with $2\text{K} \times 2\text{K}$ pixels each with a field of view of 0.763×0.722 deg^2. The 18 micron pixels correspond to an NIR plate scale of 0.30 arcsec per pixel. Spectroscopy for the BAO survey will be done with a slitless grism spectrometer using the NIR detectors with a resolution of $R = 250$.

The survey strategy is planning on a wide and a deep survey. The wide survey is expected to cover 15,000 deg^2 with a depth sensitivity of 24.5 mag in the visible imager and 24.0 mag in the NIR imager. The deep survey is expected to cover 40 deg^2 with a sensitivity two magnitudes deeper than the wide survey.

WL survey uses the 15,000 square degrees of the wide survey with a single filter band equivalent to the $R + I + Z$ filters from 550 to 900 nm. The expectation is 30 resolved galaxies per arcmin^2 with photometric redshifts with a precision of $0.05(1 + z)$. The BAO survey uses the slitless grism spectrometer with a resolution of 250, yielding a redshift precision of $0.001(1 + z)$ for $H\alpha$ emission line galaxies. The limiting line flux will be 3×10^{-16} ergs/sec/cm^2, yielding an expected 50 million galaxy redshifts with a completeness higher than 45% in the redshift range of $0.7 < z < 2.0$.

6.2.2. *WFIRST*

WFIRST[51] is a NASA space mission, with an expected international collaboration. It was first proposed as SNAP (Super Nova Acceleration Probe), was later renamed JDEM (Joint Dark Energy Mission) and finally christened WFIRST (Wide Field Infra Red Survey Telescope) by the 2010 decadal survey New Worlds, New Horizons, which recommended it as the highest priority large US space mission. A Science Definition Team has been commissioned by NASA to design the mission. The current design, described in the WFIRST-AFTA Design Report,[51] is based on a telescope with a 2.4 m primary mirror. The single imager will consist of 18 HgCdTe detectors (H4RG's) with $4\text{K} \times 4\text{K}$ pixels each. The 10 micron pixels translate into a plate scale of 0.11 arcsec per pixel. The imager will have a field of view of 0.28 sq deg with a wavelength sensitivity of 0.6 to 2.0 μ and a depth sensitivity of 27.1 mag in a 1000 sec exposure. There will be a filter wheel with six color filters and a grism with $R = \lambda/\Delta\lambda = 600$ for the BAO survey. For supernova spectroscopy there will be an Integral Field Spectrometer (IFU) with an $R = 100$.

The supernova survey will be carried out over a two year period with 30 hour observations with a five day cadence. The imager will be used to discover supernovae by repeatedly scanning up to 27 deg^2. The lightcurves will be obtained from the IFU spectrometer, significantly reducing systematic errors. A total of 2700 Type 1a supernova are expected with redshifts up to $z = 1.7$. The current plan anticipates an additional ground based sample of 800 nearby supernovae with $z < 0.1$ to anchor the Hubble diagram.

The BAO survey will use the slitless grism on the filter wheel and the imager to carry out a 2000 deg^2 galaxy redshift survey, with a sensitivity of 1.0×10^{-16} ergs/sec/cm^2. This is expected to produce 20 million Hα galaxies with $1 < z < 2$, and 2 million OII galaxies with $2 < z < 3$. The redshift precision will be $0.001(1 + z)$.

WL survey images 2000 deg^2 using the imager with four color filters. With an expected 65 resolved galaxies per arcmin^2 this will yield 500 million galaxies.

Table 10. Expected precision at the end of the dark energy program outlined above, from Weinberg *et al.*[41]

Parameter	Best estimate	Optimistic
H_0 (km/sec/Mpc)	0.40	0.26
w_p	0.011	0.008
w_a	0.11	0.07
$w(z > 1)$	0.050	0.035
Ω_k	0.00055	0.00055
$\Delta\Upsilon$	0.034	0.023

Photometric redshifts, with either ground based or IFU training, are forecast to have a precision of $0.04(1 + z)$.

6.3. *Anticipated results after the planned program*

An estimate of the precision achievable at the end of the planned program outlined above has been carried out in a comprehensive review paper by Weinberg *et al.*[41] Included in their estimate are the anticipated Supernova, the BAO, WL, and the WMAP CMB results. A short summary of their results is shown in Table 10. The second column presents the best estimates of the results of each technique combined. The third columns gives an optimistic estimate of the precision where the errors on the three dark energy technique results have been reduced by a factor of two, to give a feeling of the sensitivities. In these estimates, w_p is the width of the error ellipse in the w_a versus w_0 plane at $w_a = 0$. Because of the inclination of the error ellipse the actual error on w_0, is about three times the error on w_p. The error on $w(z > 1)$ is the error on w if the z dependence of w is evaluated in two redshift bins, $w < 1$ and $w > 1$.

The anticipated precision at the end of the planned program discussed above represent a factor of five to ten improvement over the present knowledge summarized in Table 7 above. This improvement will allow sharper distinctions about the underlying cause of the acceleration of the universe and the nature of dark energy. However there might be surprises, as there have been in the past, that could change our view of cosmology and how we define the relevant parameters that characterize it.

7. Conclusions

A vigorous program of surveys has followed the discovery that the expansion of the universe is accelerating. An impressive set of measurements of the relevant cosmological parameters have been achieved, as summarized in Table 7 above. Most of the parameters are at the few percent level of precision. The era of precision cosmology is indeed setting in. The main exception to this are the dark energy equation of state parameter w and its time dependent part w_a, which are very poorly constrained at this time. A very ambitious program of future surveys is planned

for the coming decade. The expectation is that this planned program will allow a distinction between dark energy being related to the cosmological constant or some other new constituent of the universe, or alternately the apparent acceleration of the universe has its explanation in some modification of GR.

Acknowledgments

The author thanks Professor Nikhil Padmanabhan and Professor Jack Sandweiss for a careful reading of this manuscript and for making many excellent suggestions that improved the text considerably. The author also acknowledges the comprehensive review articles by Weinberg *et al.*[41] and by Allen *et al.*[52] that helped clarify many issues relevant to this review.

References

1. A. Riess *et al.*, *Astron. J.* **116** (1998) 1009.
2. S. Perlmutter *et al.*, *Astrophys. J.* **517** (1999) 565.
3. E. Linder, *Phys. Rev. D* **72** (2005) 043529.
4. M. Phillips *et al.*, *Astrophys. J.* **413** (1993) L105.
5. P. Nugent *et al.*, *Astrophys. J.* **455** (1995) L147.
6. A. Goobar and S. Perlmutter, *Astrophys. J.* **450** (1995) 14.
7. D. Eisenstein *et al.*, *Astrophys. J.* **633** (2005) 560.
8. D. Eisenstein *et al.*, *Astrophys. J.* **664** (2007) 675.
9. N. Padmanabhan *et al.*, *Mon. Not. R. Astron. Soc.* **427** (2012) 2132.
10. F. Simpson *et al.*, *Mon. Not. R. Astron. Soc.* **429** (2013) 2249.
11. J. R. Gott *et al.*, *Astrophys. J.* **194** (1974) 543.
12. J. Bahcall *et al.*, *Astrophys. J.* **504** (1998) 1.
13. N. Kaiser, *Mon. Not. R. Astron. Soc.* **227** (1987) 1.
14. W. J. Percival and M. White, *Mon. Not. R. Astron. Soc.* **393** (2009) 297.
15. M. White *et al.*, *Mon. Not. R. Astron. Soc.* **397** (2009) 1348.
16. R. Amanullah *et al.*, *Astrophys. J.* **716** (2010) 712.
17. W. M. Wood-Vasey *et al.*, *Astrophys. J.* **666** (2007) 694.
18. A. Conley *et al.*, *Astrophys. J. Suppl.* **192** (2011) 1.
19. A. Riess *et al.*, *Astrophys. J.* **659** (2007) 98.
20. N. Suzuki *et al.*, *Astrophys. J.* **746** (2012) 85.
21. H. Campbell *et al.*, arXiv: 1211.4480.
22. R. Shrinivas *et al.*, *Publ. Astron. Soc. Pac.* **121** (2009) 1395.
23. C. Contreras *et al.*, *Astron. J.* **139** (2010) 519.
24. C. Baltay *et al.*, *Publ. Astron. Soc. Pac.* **125** (2013) 683.
25. S. C. Keller *et al.*, *Publ. Astron. Soc. Aust.* **24** (2007) 1.
26. http://pan-starrs.ifa.hawaii.edu
27. F. Beutler *et al.*, *Mon. Not. R. Astron. Soc.* **416** (2011) 3017.
28. C. Blake *et al.*, *Mon. Not. R. Astron. Soc.* **415** (2011) 2892.
29. L. Anderson *et al.*, *Mon. Not. R. Astron. Soc.* **427** (2012) 3435.
30. E. Huff *et al.*, arXiv: 1112.3143.
31. J. Benjamin *et al.*, *Mon. Not. R. Astron. Soc.* **431** (2013) 1547.
32. M. Kilbinger *et al.*, *Mon. Not. R. Astron. Soc.* **430** (2013) 2200.
33. T. Kitching *et al.*, arXiv:1401.6842.
34. M. J. Jee *et al.*, *Astrophys. J.* **765** (2013) 74.

35. H. Lin *et al.*, *Astrophys. J.* **761** (2012) 15.
36. S. W. Allen *et al.*, *Mon. Not. R. Astron. Soc.* **383** (2008) 79.
37. S. Ettori *et al.*, *Astron. Astrophys.* **501** (2009) 61.
38. A. Vikhlinin *et al.*, *Astrophys. J.* **692** (2009) 1060.
39. A. Mantz *et al.*, *Mon. Not. R. Astron. Soc.* **406** (2010) 1759.
40. M. Sullivan *et al.*, *Astrophys. J.* **737** (2011) 102.
41. D. Weinberg *et al.*, *Phys. Rep.*, in press (2013), arXiv: 1201.2434.
42. E. Komatsu *et al.*, *Astrophys. J. Suppl.* **192** (2011) 18.
43. A. Riess *et al.*, *Astrophys. J.* **730** (2011) 119.
44. S. Weinberg, *Rev. Mod. Phys.* **61** (1989) 1.
45. G. Bernstein *et al.*, *Astrophys. J.* **753** (2012) 152.
46. G. Hill *et al.*, *New Astron. Rev.* **50** (2006) 378.
47. DESI Conceptual Design Report (2013).
48. LSST Science Book, arXiv:0912.0201.
49. Z. Ma, G. Bernstein *et al.*, *Publ. Astron. Soc. Pac.* **120** (2008) 1307.
50. Euclid Red Book, ESA/SRE (2011) 12.
51. WFIRST-AFTA Final Report, NASA May 13, 2013.
52. S. W. Allen *et al.*, *Annu. Rev. Astron. Astrophys.* **49** (2011) 409.